POINT CLOUDS OVER TETIAROA – 3D MODELING OF A TROPICAL ISLAND BY TOPO-BATHYMETRIC LIDAR

Serkan Ural (1), Armin Gruen (1), Sultan Kocaman (2)

[1] Institute for Theoretical Physics, ETH Zurich, 8093 Zurich, Switzerland

[2] Hacettepe University, Dept. of Geomatics Engineering, 06800 Ankara, Turkey
Email: sural@phys.ethz.ch; agruen@geod.baug.edu.tr; sultankocaman@hacettepe.edu.tr

KEY WORDS: tropical island, bathymetry, airborne Lidar, 3D modeling

ABSTRACT: A topo-bathymetric Lidar acquisition of the Tetiaroa atoll was carried out as part of the Moorea IDEA project in May 2017. A point cloud of approximately 1.4 billion points with an average point density of 25 pt/m^2 was derived from the acquisition with a Riegl LMS-VQ820G full-waveform green Lidar system mounted on a Eurocopter AS350 at 500 m flight altitude in 32 parallel and two cross-strips covering an area of approximately 38 km^2. The accuracy has been checked with some checkpoints in open terrain. In vertical direction the mean, standard deviation, and RMSE(z) resulted in 0.04m/0.03m/0.06m respectively. The horizontal accuracy (mean, standard deviation, and RMSE) resulted in 0.04m/0.09m/0.10m and 0.02m/0.13m/0.13m in x and y components respectively.

One Pleiades 1A image triplet was also acquired in June 2014 for modeling Tetiaroa atoll. Each image of the triplet contains 4 multispectral (RGB and NIR) bands and one Panchromatic (PAN) band with an average GSD of 2.04 m and 0.51 m respectively as provided in their metadata by the vendor. The primary level (geometrically unprocessed) images (one triplet) with RPC files were provided by the satellite vendor and the geolocation accuracy was improved up to 1 pixel with an affine correction using the GCPs collected from Lidar intensity images. After the RPC improvement, a DSM of the island was produced using automatic multi-image matching.

This paper presents some of the aspects and issues regarding the quality control, blunder-detection, editing, generation of elevation models, and information extraction (vegetation, buildings, etc.) from the topo-bathymetric Lidar point cloud of Tetiaroa. In addition, we provide an analysis of the comparison of the DSM generated from the Pleiades images with that derived from Lidar data.

1. INTRODUCTION

The Moorea Island Digital Ecosystem Avatar (IDEA) project has been initiated in 2013 to build a virtual representation of Moorea Island, which can serve as model for data acquisition, data processing and simulations for tropical islands in general (Davies et. al., 2016, Cressey, 2015). The project aims to model an entire ecosystem incorporating observations, experiments, existing data and theory from different sources in various ways across a coupled 3D marine-terrestrial landscape. Tetiaroa Island in the Windward Island Group of French Polynesia is also being modeled as part of the project. Accurate 3D modeling of the land and underwater surfaces is an essential component in this effort. Recent advances and the increased availability of airborne bathymetric Lidar systems resulted with wider adoption of the technology for modeling land and underwater surfaces together (Mandlburger, 2015). Bathymetric Lidar stands out as a reliable method for nearshore and shallow coastal areas without a restriction in minimum depth that limits the use of sonar measurements at shallow waters. Alternatively, estimating the bathymetry from aerial images provides much denser sampling and better radiometric and spectral information but lacks the instantaneous 3D geometric accuracy of Lidar. Lidar is also not affected by the requirement of robustly identifiable features over the water that are crucial for image matching in photogrammetry. The utility of bathymetric Lidar especially for shallow-water coastal environments is well demonstrated (Guenther et. al., 2000; Mandlburger, 2015; Zhao et. al., 2017).

A topo-bathymetric Lidar acquisition of the Tetiaroa atoll was carried out as part of the Moorea IDEA project with the main consideration of providing a reliable and high-resolution bathymetry in the atoll, which will be used to facilitate research activities.

The Moorea IDEA project includes a number of other image-based measurement and modeling efforts, including UAV and underwater imagery. Reports on these activities are available elsewhere (Guo et. al., 2016; Gruen et. al., 2017; Neyer et. al., 2018; Nocerino et. al., 2019; Capra et. al., 2017).

2. TOPO-BATHYMETRIC LIDAR DATA AND QUALITY CONTROL

2.1 Lidar Data Acquisition over Tetiaroa

The topo-bathymetric airborne Lidar survey of Tetiaroa atoll was carried out on May 18, 2017 by Artescan - 3D Scanning, Lda. with a full-waveform 532 nm green laser Riegl LMS-VQ820G Lidar system. Aerial images with a medium format Hasselblad H50 camera were also simultaneously acquired. Both systems were mounted on a Eurocopter AS350 platform. The acquisition was completed in two flights at 500 m flight altitude covering approximately 38 km^2 in area with 32 parallel strips having 50% overlap as well as two cross-strips (Artescan, 2018). Figure 1 shows an overview of Tetiaroa and the trajectories of the two flights. The parameters for Riegl LMS-VQ820G for the airborne Lidar data acquisition of Tetiaroa are provided in Table 1.

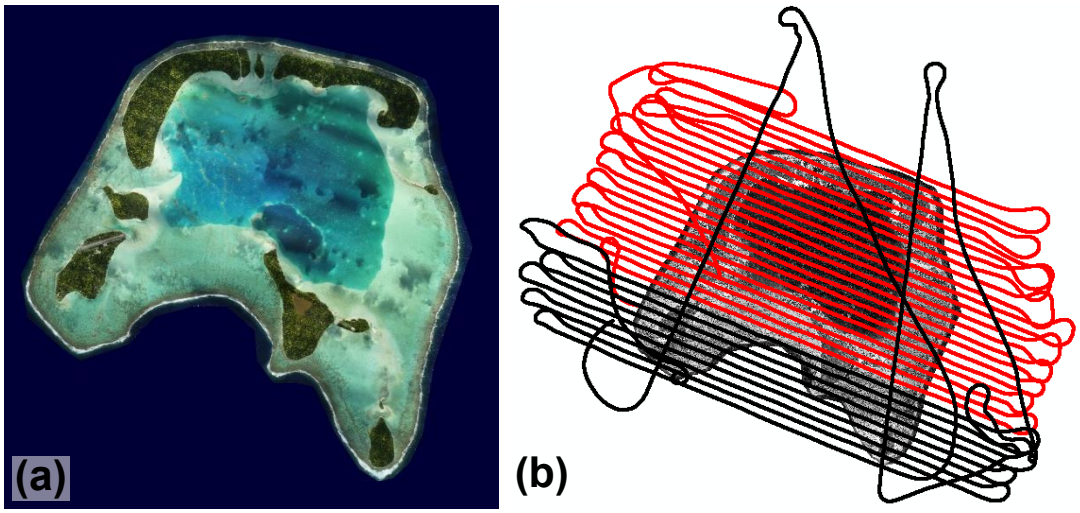

Figure 1. (a) Overview of Tetiaroa generated by 3D rendering of Lidar point cloud with RGB color information from Hasselblad images. (b) Trajectories of the two flights distinguished with different colors for airborne topo-bathymetric Lidar acquisition of Tetiaroa atoll, May 18, 2017.

The data provider performed the analysis of the full-waveform Lidar data along with georeferencing and strip adjustment. The total number of raw points is reported as approximately 1.7 billion. 3D point clouds of approximately 1.42 billion points in RGPF UTM 6S coordinate system were provided in 186 tiles of 500 m x 500 m in las format. The points were classified into five categories. Approximately, 46 million points were classified as ground, 327 million as non-ground (including vegetation, buildings and other points on land), 389 million as water surface, 628 million as lagoon bottom and seabed, and 32 million as other underwater points.

Table 1. Parameters for Riegl LMS-VQ820G for the airborne Lidar data acquisition of Tetiaroa (Actual average point density and the strip overlap map is provided in the Quality Control section)

PARAMETER	VALUE
FOV	42°
PRR	522 kHz
Beam divergence	1 mrad
Flight altitude	500 m
Point density (single strip)	15 pts/m2
Point spacing (single strip)	30 cm
Strip width	380 m
Footprint diameter	0.5 m

The Hasselblad images have approximately 75MB each and a footprint of 6 cm.

2.2 Quality Control

We performed a series of quality control stages to check the acquired Lidar point clouds for completeness, consistency, and integrity with respect to the file format, number of points, flight strips, return numbers, point density distribution,

horizontal and vertical accuracy, and classification. In this section we present these stages and some of the issues that we encountered during quality control to demonstrate that some issues ranging in significance from conventional preference to possible data corruption are identified and captured through this process.

We checked the las file versions and other metadata including the total point counts, return counts, classification counts, scale factors, coordinate offsets, tile bounding boxes, coordinate system information recorded in the las file headers for completeness and consistency. We reduced the scale factors of all v1.2 las files to 0.01 for compression efficiency since they were one order of magnitude higher than the acquisition precision. The las files included records containing up to 7 returns. The point counts for the sixth and seventh returns were not recorded in the header files due to the limitation of this version of the las format. We removed an offset of 6,000,000 that we have observed in all header files since it was a divergence from the standard coordinate reference system definition and affected the interoperability of the las files together with other data.

In order to check for completeness, we created a flight-strip overlap map with LASTools (2018) software. No data gaps were observed. The majority of the project area was acquired in two flight strips while some regions were covered by only one or three flight strips. We calculated the point density distribution for the project area and generated a point density map. The average point densities for all returns and last returns are 38.1 pts/m^2 and 24.9 pts/m^2 respectively. The corresponding average point spacing is approximately 16 cm for all returns and 20 cm for last returns only. Figure 2 shows the flight strip coverage and last return point density distribution maps.

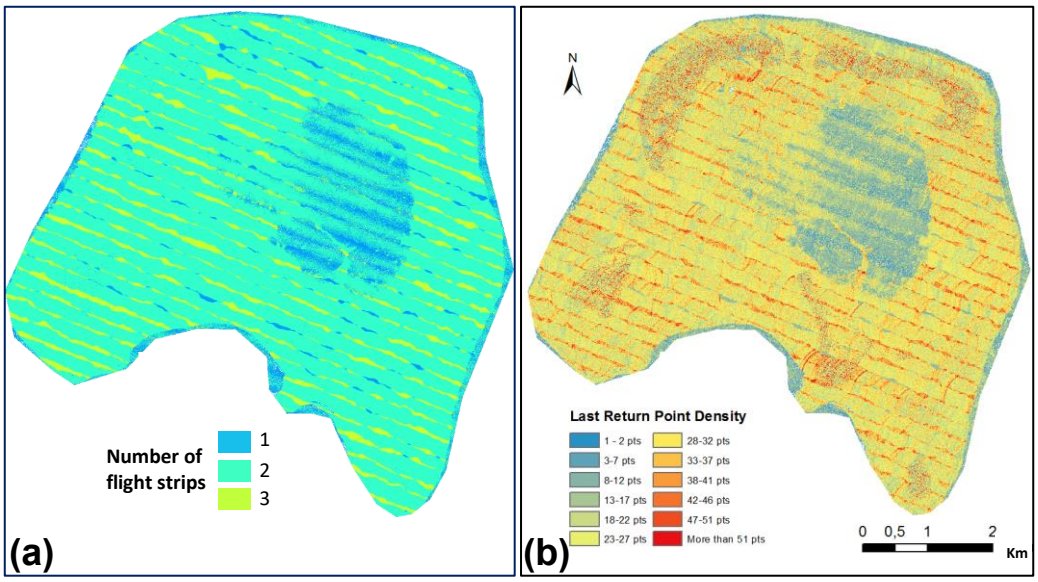

Figure 2. (a) Flight strip coverage map. (b) Last return point density distribution map.

The point density map for last returns presented an area with no points even though there were no coverage issues present. We found the gap to be due to the return number records in the las file of this area. This area included many points which were first returns that were not single returns. However, there were only few last returns that weren't single returns in the same area. It occurs that either some "last of many" returns had been removed and their corresponding first returns remained in the dataset, or the "number of returns" records of many points were recorded incorrectly. Figure 3 below shows the area for which these return number issues were identified.

Apart from the expected variation of point cloud density due to flight strip overlaps and vegetation cover, we observed several areas with higher point densities compared to their surroundings. Such deviations may be due to the fluctuations in flight parameters causing more than the planned number of Lidar pulses to be emitted to these areas.

We checked the vertical accuracy of the Lidar point cloud by calculating the elevation differences between the nine vertical reference points in open terrain that were surveyed with GPS and the local TINs generated around them using the points classified as ground. The mean, standard deviation, and the RMSE(z) are presented in Table 2. We also checked the elevation differences for the coinciding areas of adjacent strips. We calculated the strip differences with respect to the minimum elevation values of points in the ground and lagoon-bottom/seabed classes within coinciding one-meter grid cells using LASTools (2018). A strip difference map and the histogram of calculated differences within a ±1 m range are provided in Figure 4.

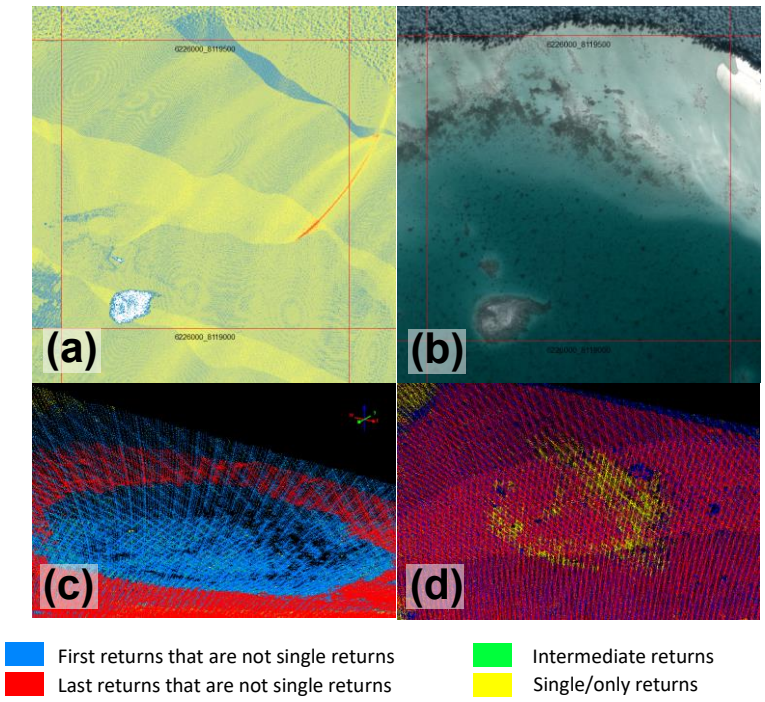

Figure 3. (a) Last return point density distribution of the tile with return number issues. (b) Pleiades image of the same area. (c) Visualization of the return numbers in the area before correction. (d) Visualization of the return numbers after correction.

Table 2. Vertical accuracy measures calculated at nine GPS surveyed check points.

Mean	0.04 m
Std. Dev.	0.03 m
RMSE(z)	0.06 m

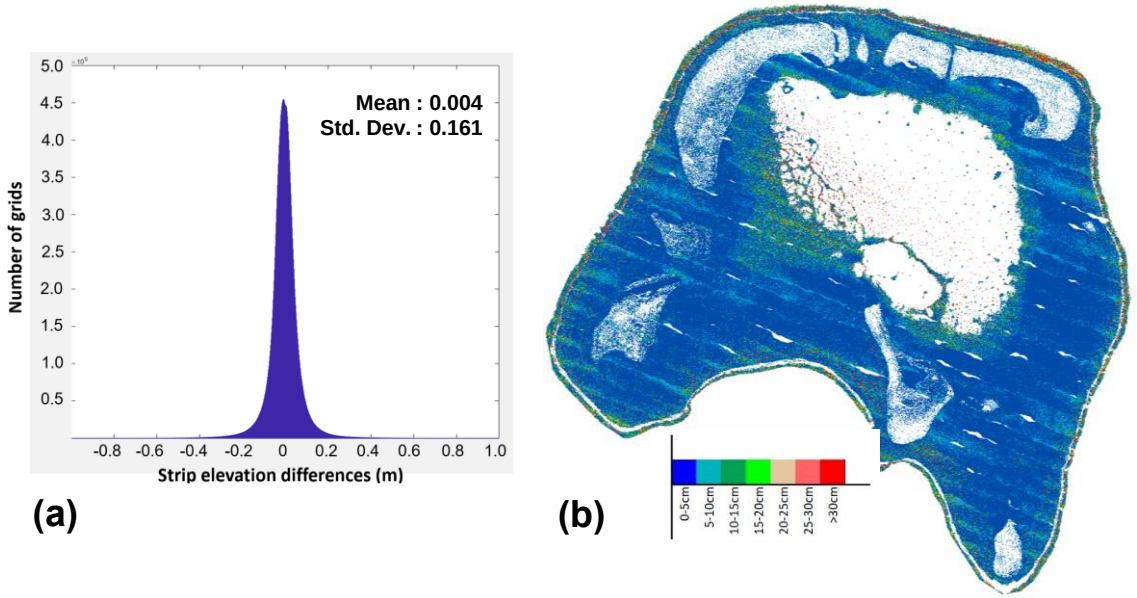

Figure 4. (a) Histogram of elevation differences within ±1m range for coinciding 1 m grid cells of adjacent strips. (b) Map of elevation differences of points classified as ground or seabed within coinciding 1 m grid cells of adjacent strips.

We checked the horizontal accuracy by comparing the GPS surveyed coordinates of seven checkpoints that are identifiable on the intensity images in open terrain resampled on a 10 cm grid by interpolating the intensity values of the points with LASTools (2018). Figure 5 shows selected checkpoints as observed on the intensity images. The

mean, standard deviation, and RMSE are calculated as 0.04m/0.09m/0.10m and 0.02m/0.13m/0.13m in x and y components respectively.

The classification of points as provided by the data provider were examined to identify any issues that may have significant effects on generating further derivatives from the Lidar data. Depending on the definition of what constitutes “ground”, the classes "ground" and non-ground" are usually self-evident on larger pieces of land even though classification may become challenging at instances of small pieces of land partially covered by water, vegetation, and/or other structures. We observed instances partially demonstrating such challenges as misclassifications throughout the dataset. Some of these include points:

- along the shoreline at the same elevation level as ground, classified as lagoon bottom/seabed surrounded by ground and off-ground points
- surrounded by lagoon bottom/seabed points with higher and lower elevation values, that are not ground but classified as such
- with elevation values lower than the water surface points around them classified as ground
- classified as water surface adjacent to ground but with elevations above ground level
- classified as lagoon bottom/seabed but are actually other points in water
- classified as ground but are actually non-ground.

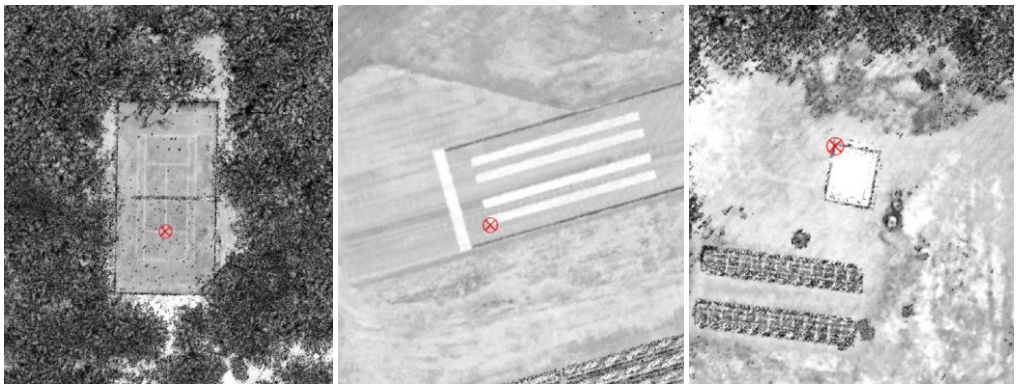

Figure 5. Selected examples of checkpoints measured on interpolated intensity images resampled from Lidar point clouds at 10cm.

3. POST PROCESSING AND DERIVATIVE PRODUCTS

3.1 Blunder Detection and Editing

In order to identify any remaining blunders in the Lidar point clouds we investigated the DTM and the DSM. We generated a 50 cm DTM from the points classified as ground and lagoon bottom/seabed by TIN interpolation using LASTools (2018). The elevations in the DTM had a minimum value of -22.12 m and a maximum value of 10.64 m. Visual inspection of the DTM and the histogram of elevations suggested that the maximum elevation values of the DTM were in the range of 5-6 m. Tiles with elevation values higher than 6 m were identified and global high blunders were removed semi-automatically. High points within the grid cells with elevation values above the threshold were identified and then removed after visual confirmation as outliers.

After the removal of global high points, we eliminated the local spikes which still remained on the DTM. Low spikes below ground were observed and high spikes that couldn’t be identified in a global detection were also confirmed later as a result of local blunder detection. One of the main reasons for such blunders was the ground filtering errors where low vegetation or other objects are misclassified as ground and not detected during manual editing of ground filtering results.

We estimated the parameters of a second order surface polynomial fit on a moving window over a 30 cm minimum elevation grid and calculated the residuals for each grid cell to identify and remove local blunders. A semi-automatic approach for editing the blunders by utilizing the residual statistics were preferred due to the characteristics of some blunders observed in the dataset. We investigated the residuals of the polynomial surface fit by their magnitude. Starting with the group of residuals with the largest magnitude, we removed the points in the grid cells with residuals that we visually identified as local outliers from the ground or lagoon bottom/seabed class. Figure 6 shows examples of outliers that were removed.

A typical occurrence of outliers was due to the non-smooth morphology of the forereef. This type of blunders is challenging to identify fully automatically due to the non-smooth surface structure. Another notable category of blunders was due to groups of points in the water possibly resulting from schools of fish. We also observed instances underwater where there are circular patches with no data of the lagoon bottom with single or few points that are blunders closer to the water surface. There are no Lidar returns for most part from these small patches that correspond to some darker colored areas under water. These areas are different in texture from their immediate environment on the orthophotos. Some similar darker patches in the images around these no-data areas occur as rocks/corals in the Lidar data. Not all of these patches involve blunders. Some have no points up to the sea surface while groups of points that appear to be part of a rock/coral exist within these circular, otherwise empty patches. It is likely that the material characteristics of these structures combined with water depth results in no or limited Lidar return echoes. The instances we observed were approximately -7m and below in depth.

For identifying the high global blunders in the DSM, we calculated the height of each point with respect to the local ground surface and generated a 1m grid of highest point heights. Several instances of very high points were identified and removed from the dataset.

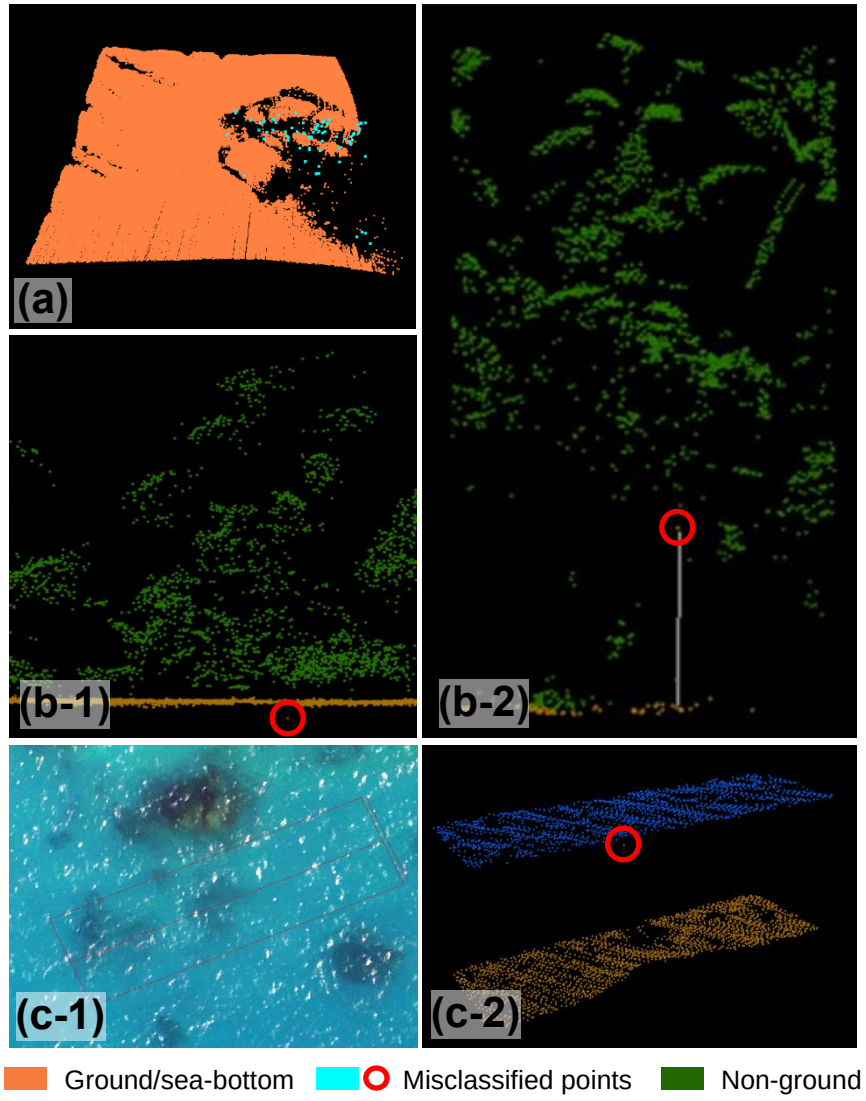

Figure 6. Selected examples of removed blunders in lagoon bottom (a, c-2), and ground points (b-1, b-2). The orthophoto corresponding to the area of the blunder in (c-2) is presented in (c-1).

3.2 DTM and DSM Generation

After the identification and removal of blunders, we generated a 30 cm DTM by TIN interpolation using LASTools (2018). We also generated a DSM with the same ground sampling distance as a highest point grid. Figure 7 presents visualizations of the DTM and the DSM.

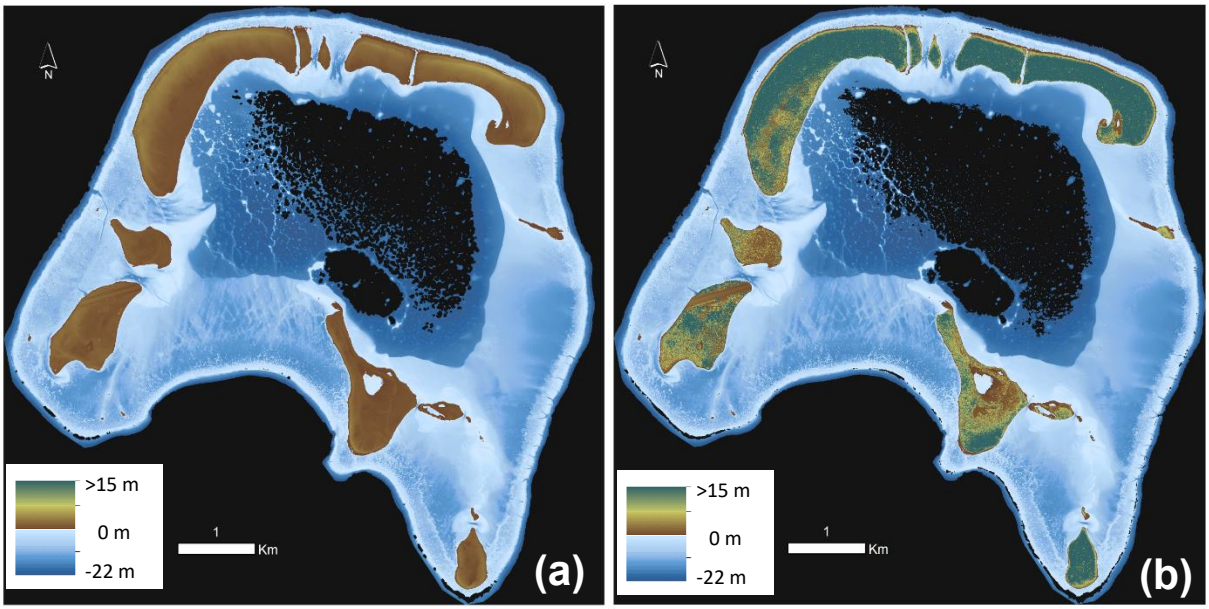

Figure 7. 30 cm DTM (a) and DSM (b) of Tetiaroa atoll generated from topo-bathymetric Lidar point clouds.

3.3 Classification of Buildings and Other Man-Made Structures

We classified the buildings in Tetiaroa which are mainly concentrated on Onetahi motu by clustering co-planar points using Lidar 360 (2018) software. Local surface normals, min/max building size, and max surface slope were considered for identifying points that form building roofs. Building classification results serve two main purposes: The first one is building modeling. The second purpose is the separation of vegetation points from the building points and from other structures so that a reliable vegetation analysis can be performed without their influence.

The results of automatic building classification included misclassifications that required manual editing. In case of misclassification of trees as buildings, errors were mainly due to dense vegetation for which the point sampling formed surfaces that were mistaken as building roofs. Another category was when the trees overhanging over the roofs were too close to the roofs. In these cases, either parts of building roofs were included in the vegetation class or parts of trees were included in the building class as an extension of the roof by the software.

Apart from the buildings, some other man-made structures that are not buildings were also either classified as buildings or vegetation. We manually edited the building classification results to acquire a classification that would allow the removal of buildings and other structures for reliable vegetation analysis. Figure 8 provides color-coded classification results from Onetahi motu where almost all buildings are located.

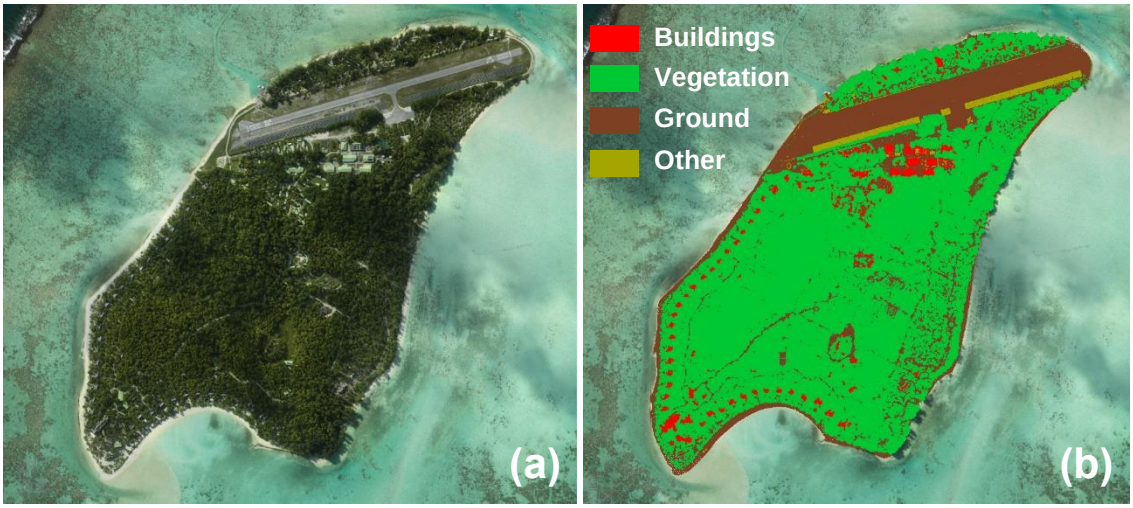

Figure 8. Orthophoto mosaic (a), and building classification results (b) superimposed on the orthophoto mosaic of Onetahi motu

4. COMPARISON OF LIDAR AND SATELLITE DERIVED DSMs

One Pleiades 1A image triplet (Airbus Defense and Space, 2019) was acquired in June 2014 for modeling Tetiaroa atoll. Each image of the triplet contains 4 multispectral (RGB and NIR) bands and one Panchromatic (PAN) band with an average GSD of 2.04 m and 0.51 m respectively as provided in their metadata by the vendor. The primary level (geometrically unprocessed) images (one triplet) with RPC files were provided by the satellite vendor and the geolocation accuracy has been improved up to 1 pixel with an affine correction using the GCPs collected from Lidar intensity images. After the RPC improvement, a DSM of the island was produced using automatic multi-image matching.

We compared the underwater parts of the DSM point cloud generated from Pleiades image triplets using IMAGINE Photogrammetry (2018) software (DSM-P) with the underwater parts of the Lidar point cloud (DSM-L). We calculated the 3D distances between them with the Multiscale Model to Model Cloud Comparison method as implemented by M3C2 plugin (Lague et. al., 2013) in CloudCompare (2019) software. We applied an iterative closest point (ICP) registration to the Pleiades point clouds considering the Lidar point cloud as reference to account for the remaining misalignment using CloudCompare. We first generated a land mask and separated the points that are on land and the points that are underwater so that the transformation is not influenced by the refraction and other issues affecting the photogrammetric model for underwater points. We also reduced the number of points in the Lidar point cloud by subsampling with 1m radius by a variant of Poisson disk sampling algorithm (Cline et. al., 2009) as implemented in pdal Point Data Abstraction Library (PDAL Contributors, 2019). Then we applied ICP registration with CloudCompare (2019) software using the Pleiades and Lidar land points. The rotation and translation parameters resulting from the ICP registration are provided in Table 3.

Table 3. Rotation and translation parameters resulting from ICP registration between Pleiades and Lidar land points

Rotation			**Translation (m)**
1	0.000008	-0.000056	-0.02
-0.000008	1	0.000006	-0.14
0.000056	-0.000006	1	-0.90

We applied the transformation to remaining Pleiades underwater points using the transformation parameters estimated with ICP registration. After having the two point clouds aligned, we calculated the point distances between the Pleiades underwater point cloud and the subsampled underwater Lidar point cloud. Figure 9 provides the histogram of calculated differences, difference statistics and the difference map.

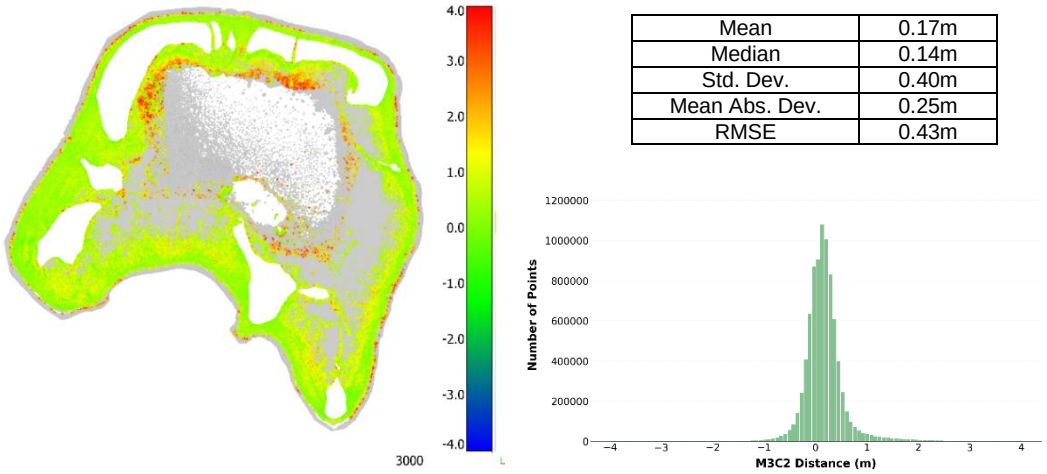

Figure 9. Left: Map of M3C2 distances calculated between DSM-P and DSM-L. The color ramp represents distances in meters saturated at ±4m. Grey color indicates "no correspondence" of Lidar points in the Pleiades point cloud. Top right: Statistics for calculated distances. Bottom right: Histogram of calculated distances.

Refraction is one of the main contributors to the errors affecting the photogrammetric models underwater. Without any refraction correction, one would expect to see a trend in the calculated differences between the two bathymetric surfaces derived from Lidar and satellite photogrammetry as a function of depth due to refraction. This is clearly observed in the scatter plot of depth vs. distance for the calculated distances between the Lidar and Pleiades DSM provided in Figure 10. The calculated difference presents a major trend as a function of depth along with a large variation around this trend as observed in the figure.

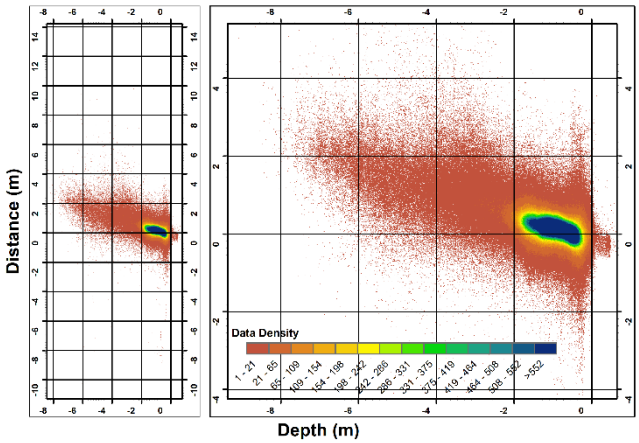

Figure 10. Overview (left) and detail (right) scatter plots of calculated differences between DSM-L and DSM-P wrt. water depth. Data density color ramp represents density ranges for the number of points per unit plot area (1cm x 1cm).

5. CONCLUSIONS

We presented the topo-bathymetric Lidar data of Tetiaroa acquired for the Moorea IDEA project along with some of the aspects and issues regarding the quality control, blunder-detection, editing, generation of elevation models, and information extraction. In addition, we provided the comparison of the DSMs generated from the Pleiades images with that derived from Lidar data of Tetiaroa.

The specifications of the topo-bathymetric Lidar data of Tetiaroa allows it to be utilized for a variety of applications including coral mapping, turbidity studies, understory vegetation characterization, turtle nest monitoring, modeling of mosquito spatial dynamics, sea level monitoring, tidal analysis and beach flooding pattern research, and integration with bathymetry from other sources among others.

Regardless of how well the Lidar point cloud is classified using automatic filtering and classification algorithms, manual editing is usually required to have a clean, reliable Lidar dataset. This aspect is often not emphasized enough even though researchers spend a significant amount of time on such efforts. 3D visualization and editing tools are two important aspects of post-processing Lidar data open to improvement for intuitive and fast editing processes.

Comparison of the bathymetry derived from Lidar and Pleiades images of Tetiaroa showed that the differences between the two surfaces present a relation to depth, which is observed clearly in shallow water down to the range of approximately -7m. However, the majority of the points in the Pleiades DSM are concentrated in the shallow depth ranges. The Pleiades DSM is not available with dense sampling within the entire depth range where Lidar data is available. This limits the comparison mostly to the very shallow parts of the lagoon. Further study is required for a more detailed analysis for characterizing the significance of and the variation around the observed trend.

ACKNOWLEDGEMENTS

We especially would like to thank Prof. Matthias Troyer for his financial and scientific support provided through the Institute of Theoretical Physics, ETH Zurich. The research was executed under permits issued by the French Polynesian Government (Délégation à la Recherche) and the Haut-Commissariat de la République en Polynésie Francaise (DTRT) (Protocole d'Accueil 2005-2018). The authors would like to thank Dr Erica Nocerino (ETH Zurich) for her support and useful discussions.

REFERENCES

Airbus Defense and Space, 2019. Pleiades. Retrieved from http://www.intelligence-airbusds.com/files/pmedia/public/r61_9_geo_011_pleiades_en_low.pdf

Artescan 3D Scanning, Lda., 2018. Topo-Bathymetric LiDAR Survey Tetiaroa Atoll/Tahiti Final Report.

Capra, A., Castagnetti, C., Dubbini, M., Gruen, A., Guo, T., Mancini, F., Neyer, F., Rossi, P., Troyer, M., 2017. High accuracy underwater photogrammetric surveying. In: Proceedings of 3rd IMEKO International Conference on Metrology for Archaeology and Cultural Heritage, MetroArcheo 2017, p. 696-701, ISBN: 978-92-990084-0-9, Lecce, Italy, 23-25 October 2017.

Cline, D., Jeschke, S., White, K., Razdan, A., Wonka, P., 2009. Dart throwing on surfaces. Comput. Graph. Forum 28, 1217–1226. https://doi.org/10.1111/j.1467-8659.2009.01499.x

CloudCompare (version 2.10.2) [GPL software], 2019. Retrieved from http://www.cloudcompare.org/
Cressey, D. 2015. Tropical paradise inspires virtual ecology lab. Nature 517: 255–256. doi:10.1038/517255a.

Davies, N., Field, D., Gavaghan, D., Holbrook, S.J., Planes, S., Troyer, M., Bonsall, M., Claudet, J., Roderick, G., Schmitt, R.J., Zettler, L.A., Berteaux, V., Bossin, H.C., Cabasse, C., Collin, A., Deck, J., Dell, T., Dunne, J., Gates, R., Harfoot, M., Hench, J.L., Hopuare, M., Kirch, P., Kotoulas, G., Kosenkov, A., Kusenko, A., Leichter, J.J., Lenihan, H., Magoulas, A., Martinez, N., Meyer, C., Stoll, B., Swalla, B., Tartakovsky, D.M., Murphy, H.T., Turyshev, S., Valdvinos, F., Williams, R., Wood, S., 2016. Simulating social-ecological systems: The Island Digital Ecosystem Avatars (IDEA) consortium. Gigascience 5, 1–4. https://doi.org/10.1186/s13742-016-0118-5

Gruen, A., Kocaman, S., Guo, T., Ural, S., Troyer, M., 2017. DSM / DTM - related investigations of the Moorea Avatar project. 38th Asian Conf. Remote Sens. - Sp. Appl. Touching Hum. Lives, ACRS 2017 23–27.

Guenther, G.C., Cunningham, A.G., LeRocque, P.E., Reid, D.J., 2000. Meeting the accuracy challenge in airborne lidar bathymetry, In: Proceedings of EARSeL-SIG-Workshop LIDAR. pp. 1–28.

Guo, T., Capra, A., Troyer, M., Gruen, A., Brooks, A.J., Hench, J.L., Schmitt, R.J., Holbrook, S.J., Dubbini, M., 2016. Accuracy assessment of underwater photogrammetric three dimensional modelling for coral reefs. Int. Arch. Photogramm. Remote Sens. Spat. Inf. Sci. - ISPRS Arch. 41, 821–828. https://doi.org/10.5194/isprsarchives-XLI-B5-821-2016

IMAGINE Photogrammetry [Computer Software], 2018. Hexagon Geospatial.

Lague, D., Brodu, N., Leroux, J., 2013. Accurate 3D comparison of complex topography with terrestrial laser scanner: Application to the Rangitikei canyon (N-Z). ISPRS J. Photogramm. Remote Sens. 82, 10–26. https://doi.org/10.1016/j.isprsjprs.2013.04.009

LAStools (version 190507, academic) [Computer Software], 2018. Retrieved from http://rapidlasso.com/LAStools

Lidar 360 (version 2.2., trial) [Computer Software], 2018. GreenValley International. Retrieved from https://greenvalleyintl.com/software/lidar360/

Mandlburger, G., Hauer, C., Wieser, M., Pfeifer, N., 2015. Topo-bathymetric LiDAR for monitoring river morphodynamics and instream habitats-A case study at the Pielach River. Remote Sens. 7, 6160–6195. https://doi.org/10.3390/rs70506160

Neyer, F., Nocerino, E., Gruen, A., 2018. Monitoring coral growth - The dichotomy between underwater photogrammetry and geodetic control network. Int. Arch. Photogramm. Remote Sens. Spat. Inf. Sci. - ISPRS Arch. 42, 759–766. https://doi.org/10.5194/isprs-archives-XLII-2-759-2018

Neyer, F., Nocerino, E., Gruen, A., 2019. Image quality improvements in low-cost underwater photogrammetry. ISPRS Ann. Photogramm. Remote Sens. Spat. Inf. Sci. 42, 135–142. https://doi.org/10.5194/isprs-archives-XLII-2-W10-135-2019.

Nocerino, E., Neyer, F., Gruen, A., Troyer, M., Menna, F., Brooks, A., Capra, A., Castagnetti, C., Rossi, P., 2019. Comparison if diver-operated underwater photogrammetric systems for coral reef monitoring. ISPRS Ann. Photogramm. Remote Sens. Spat. Inf. Sci. 42, 143–150. https://doi.org/10.5194/isprs-archives-XLII-2-W10-143-2019

PDAL Contributors, 2018. PDAL Point Data Abstraction Library. doi:10.5281/zenodo.2556738

Zhao, J., Zhao, X., Zhang, H., Zhou, F., 2017. Improved model for depth bias correction in airborne LiDAR bathymetry systems. Remote Sens. 9, 1–16. https://doi.org/10.3390/rs9070710